Locomotion Optimization of a Tendon-Driven Robotic Fish with Variable Passive Tail Fin

Changlin Qiu, *Student Membership*, Zhengxing Wu, *Senior Member, IEEE*, Jian Wang, *Membership*, Min Tan, *Membership*, and Junzhi Yu, *Fellow, IEEE*

***Abstract*—This paper explores a set of locomotion optimization methods for a novel tendon-driven robotic fish. With the typical features of the dual tendon driving active tail and variable stiffness passive caudal fin, a fully functioning tendon-drive robotic fish is developed. Next, a practical dynamic model for the tendon-driven robotic fish is established with full consideration of variable stiffness passive caudal fin, and the model parameters are accurately identified via data-driven methods. More importantly, to improve the motion performances, an asymmetric central pattern generator (CPG) is particularly proposed, and an adjustment rule of passive stiffness is explored to fit different motion states of the robotic fish. Finally, extensive simulations and aquatic experiments verify the feasibility of the proposed prototype and locomotion optimization methods. The obtained results show that the improvements of steering radius and forward swimming velocity are 36.3% and 29%, respectively. At present, our robotic fish can achieve maximum forward swimming as 1.04 BL/s (BL for the Body Length), maximum turning rate as 153.3°/s, and the minimum turning radius reaches to 0.31 BL, providing a valuable reference for bio-inspired research of aquatic mechanical design and locomotion control.**

***Index Terms*—Underwater robotics, robotic fish, motion control, asymmetric CPG, variable passive caudal fin.**

I. Introduction

FISH can achieve excellent maneuverability and propulsive efficiency with their bodies, tails, and fins [1], [2]. Inspired by the effective mechanical system of fishes, MIT developed the first fish-like robot – RoboTuna in 1994 [3]. In recent years, the bionic robotic fishes have been widely studied in the aspect of structural design [4], locomotion control [5], and so on. By virtue of the advantages of the remarkable efficiency, maneuverability, concealment, and biological friendliness, the robotic fishes exhibit extensive application prospects in military detection, oceanic supervision, and aquatic life-form observation [6], [7]. Therefore, the robotic fish with reasonable structure and effective control method is still a research focus in the field of underwater robotics.

For the electromechanical realization of robotic fishes, a common solution is the rigid link structure [4]. These robotic fishes have one or more rigid links and are driven by independent joints. Whereas redundant drivers and frictional losses are not conducive to the improvement of energy efficiency and extension of functionality. In some cutting-edge researches, many novel driving methods are applied into the development of robotic fish, such as magnetic drive [8] and ion polymer metal composite drive [9]. However, the problems of low maneuverability, poor efficiency, and complex processing technology still exist.

Anatomically, the fishes with the propulsion mode of "Body and/or Caudal Fin" (BCF) are made up of a central spine and muscles on both sides, which can achieve great thrust and acceleration [10]. On the basis of biology, the robotic fishes driven by the bionic tendons are proposed [11]–[14]. They are more in line with the driving patterns of real fishes. For instance, Zhong *et al.* proposed a cable-driven robotic fish that used only one servo motor to accomplish the flexible fish-like motion [15]. Similarly, Liu *et al.* developed a tendon-driven robotic dolphin termed "ContRoDolI" [16], which is equipped with a single degree of freedom (DOF) thoracic vertebra and two-DOF caudal vertebra. Moreover, the bionic tendon-driven tail can easily achieve more complex functions without redundant drivers. Li *et al.* developed a robotic fish with vector propulsion [17], which can swim like shark and/or dolphin. In the above tendon driven robotic fishes, the resilience of tail is provided by the elastic plates or rods. But their elastic characteristics are ambiguous. It makes the analysis of the tail deformation complicated.

In order to achieve more outstanding task execution, many efforts have been made to improve the performance and stability of robotic fish. In terms of locomotion control, the center pattern generator (CPG) is a biological-inspired signal generator, which is able to produce stable rhythm signals and smooth signal changes. Ijspeert *et al.* presented a signal generator model and implementation in an amphibious salamander robot, which can achieve the robot motion switch between swimming and walking [18]. The CPG is also widely used in robotic fish to support its rhythmic motion [19], [20]. However, the signals generated by above CPG are symmetrical. Thus, the CPG-

This work was supported in part by the National Natural Science Foundation of China under Grant 61725305, Grant U1909206, Grant T2121002, Grant 61973303, and Grant 62022090, in part by the Beijing Nova Program under Grant Z201100006820078, and in part by the Joint Fund of Ministry of Education for Equipment Pre-Research under Grant 8091B022134. *(Corresponding author: Junzhi Yu.)*

C. Qiu, Z. Wu, J. Wang, and M. Tan are with the State Key Laboratory of Management and Control for Complex Systems, Institute of Automation, Chinese Academy of Sciences, Beijing 100190, China, and also with the School of Artificial Intelligence, University of Chinese Academy of Sciences, Beijing 100049, China (e-mail: qiuchanglin2019@ia.ac.cn; zhengxing.wu@ia.ac.cn; jianwang@ia.ac.cn; min.tan@ia.ac.cn).

J. Yu is with the State Key Laboratory for Turbulence and Complex Systems, Department of Advanced Manufacturing and Robotics, BIC-ESAT, College of Engineering, Peking University, Beijing 100871, China, and also with State Key Laboratory of Management and Control for Complex Systems, Institute of Automation, Chinese Academy of Sciences, Beijing 100190, China (e-mail: junzhi.yu@ia.ac.cn).

based steering relies heavily on the offset of oscillation. As a result, the steering maneuverability is limited. For multimodal swimming of robotic fish, Wu *et al.* developed an improved central pattern generator (CPG) model allowing free adjustment of the phase relationship among outputs [21]. In pursuit of amazing steering, Su *et al.* [22] and Marchese *et al.* [23] achieved short-term fish-like C-shape steering with control strategy designed by human. For long-term maneuverability improvements, Li *et al.* explored an improved CPG model which can generate asymmetric oscillations [17]. But the high-order of the oscillation model makes it suffer computational burden. Thus, a low-order control strategy that can equalize steering speed and stability remains an issue.

Furthermore, the characteristics of the caudal fin have a significant impact on the performance of the robotic fish. In nature, fish can achieve efficient and maneuverable movement with the help of passive caudal fins. Inspired by the bionic propulsion, many studies have been conducted on the passive caudal fin and its enhancements have been proved experimentally and theoretically [15], [25], [28], [29]. Zhong *et al.* designed a passive tail fin for tendon-driven robotic fish and reached a maximum speed of 2.15 BL/s (BL: body length) [15]. Nevertheless, the immutable compliant structures can only improve the swimming performance in a small frequency range [24] [30]. Under the inappropriate frequencies, the effect of passive joints can even be negative. On the basis of biological researches, many variable-stiffness bionic structures are proposed [31]. Particularly, Zhong *et al.* derived a model to investigate the influence of tuning stiffness, and a speed-based stiffness adjustment rule was developed [32]. In this study, the passive caudal fin operates on a robotic fish fixed on a stand, where the motion states as velocity can be measured easily and the robotic fish does not have the ability to swim freely. Therefore, it is challenging to be applied in the situation of free swimming, because the velocity related to water is unobservable and the mechanical space of wireless robotic fish is limited. Meanwhile, the practical motion dynamic model for robotic fish with variable stiffness passive caudal fin is still inadequate. Chen *et al.* proposed a Newton-Lagrange model of passive caudal fin [25]. Nguyen *et al.* built a dynamic model for a non-uniform flexible tail which was considered as a rotary slender beam [26]. Tan *et al.* built dynamic models for two kinds of flexible joints and further analyzed the influence of joint stiffness on swimming performance [27]. In the above researches, the stiffness of passive joint is constant. The modeling of the robotic fish with the variable passive caudal fin needs further research.

In order to improve the performance of robotic fish, we propose locomotion optimization methods including an improved CPG model and variable stiffness passive caudal fin. Correspondingly, extensive experiments are conducted to verify the effectiveness of the proposed methods. The primary contributions made in this paper can be summarized as the following three aspects.

1) A fully functioning tendon-driven robotic fish with variable stiffness passive caudal fin is designed and realized. In detail, a unique tendon-driven structure with torsion springs is developed and a variable stiffness passive caudal fin is achieved by the motor and springs.
2) An improved center pattern generator called A-CPG is proposed to enhance the steering performance, where an accelerating factor is introduced to achieve an asymmetric oscillation signal.
3) A frequency-based passive stiffness adjustment rule is explored based on the dynamic model and multi-objective optimization. With the developed variable passive caudal fin and the adjustment rule, the swimming velocity and stability are obviously improved.

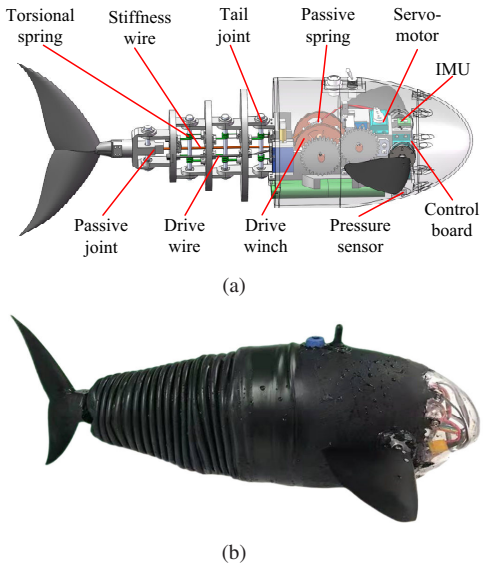

Fig. 1. The overview of "T-Fish". (a) Conceptual design. (b) Robotic prototype.

The rest of this article is organized as follows. In Section II, we propose the mechanical structure of the tendon-driven robotic fish and its variable stiffness passive caudal fin. Section III describes the process of dynamic modeling of the robotic fish and the identification of model parameters. In Section IV, an A-CPG model is presented and the passive stiffness adjustment rule is investigated. Then, simulations and experiments are carried out for verification in Section V. Finally, Section VI concludes this article.

II. Design of Tendon-Driven Robotic Fish

As illustrated in Fig. 1, a fully functioning tendon-drive robotic fish ("T-Fish") is proposed, which stands out in a new scheme of variable stiffness caudal fin in small continuous deformation robotic fish. "T-Fish" can be divided into three mechanical parts: fore body, active tail, and variable passive caudal fin. The fore body accommodates all the electrical system and drivers, and a pair of movable pectoral fins are integrated. A Cortex-M4 is employed as the micro-controller and wireless modules are applied for communication. A flexible silicone shell is used for water resistance as shown in Fig. 1(b). More detailed configurations of "T-Fish" are tabulated in Table I.

The active tail consists of a set of backbone skeleton, supporting tendons, and driving tendons. The backbone skeleton is composed of three rigid skeleton linkages hinging together end

TABLE I
DETAILED CONFIGURATIONS OF TENDON-DRIVEN ROBOTIC FISH

Items	Characteristics
Length and width	0.45 m × 0.026 m
Weight	3.6 kg
Micro-controller	STM32F407VGT6
Drive motors	Savox 125 & DG-3150
Wireless communication module	YL100 (433 MHz)
Power supply	Lipo–2S (7.4 V)
IMU	MPU6050
Depth sensor	MS5807
Extension spring	85 N/m
Torsion spring	1.15 N·m/rad

to end. Torsion springs are chosen as supporting tendons rather than elastic sheets or rods. In contrast, the spring coefficient is easy to calculate and is constant. In the developed active tail, the deformation of the tail can be calculated according to the torsion of the springs. A pair of wire ropes are fastened on the linkage at the end acting as the driving tendons of the tail. The other ends of wire ropes are wound around winches driven by a servomotor.

Specially, the variable passive caudal fin is realized by a wire rope and spring, its schematic diagram is shown in Fig. 2. The connection wire rope connects the caudal fin and passive spring, and runs through the center of the entire tail. This layout can decouple the active tail motion and passive joint rotation. When the passive joint rotates under the interaction of water, the link will drive the wire rope to translate and stretch the passive spring. Notice that the other end of the passive spring is fixed on a servomotor. In this way, the pre-tension of the passive spring can be adjusted. Then, the passive torque can be adjusted to adapt to different swimming patterns. The detailed analysis of variable passive structure can be found in Section IV. B.

III. Dynamic Modeling of the Tendon-driven Robotic Fish with Variable Passive Joint

In order to provide basis for the study of stiffness adjustment and controller design, a two-dimensional dynamic model is proposed in this section. Since the rotation of the passive caudal fin depends on complex interactions between tail-beat and hydrodynamic forces, it is difficult to accurately calculate the rotation angle of the passive joint directly. Therefore, the Lagrange dynamic modeling approach is applied to construct the dynamic model of "T-Fish".

As shown in Fig. 3, the structure of robotic fish is simplified as five links and four joints. The inertial coordinate frame is denoted as $O_w - x_w y_w z_w$. The plane $O_w x_w y_w$ coincides with horizontal plane. $O_i - x_i y_i z_i$ denotes the relative coordinate frame system attached to the link L_i, where $i \in [0, 4]$. Especially, the head link of robotic fish is indicated as L_0 and the passive caudal fin link is L_4. The setting of coordinate origin O_i can be fined in Fig. 3. All coordinate systems conform to the right hand rule.

Furthermore, some notation conventions are defined to clarify the motion states and the dynamic model. For i-th

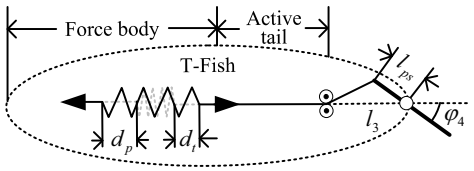

Fig. 2. The diagram of passive stiffness adjustment.

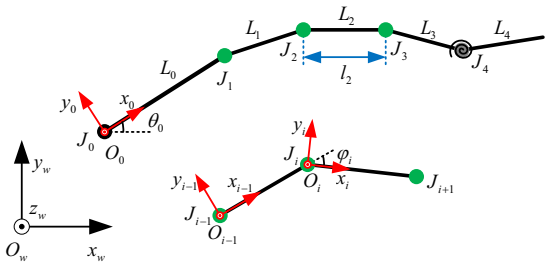

Fig. 3. The definition of the coordinate systems.

link, φ_i and θ_i denote the rotation angle of axis x_i relative to the axis x_{i-1} and the axis x_w, respectively. The linear velocity and angular velocity of L_i relative to the inertial frame system are indicated as $V_i = ({}^w v_{x,i}, {}^w v_{y,i}, {}^w v_{z,i})^T$ and $\Omega_i = ({}^w \omega_{x,i}, {}^w \omega_{y,i}, {}^w \omega_{z,i})^T$, respectively. The velocity and angular velocity in the relative coordinate system are indicated as $v_i = (v_{x,i}, v_{y,i}, v_{z,i})^T$ and $\omega_i = (\omega_{x,i}, \omega_{y,i}, \omega_{z,i})^T$, respectively.

A. Lagrange Dynamic Modeling

During modeling, the position and orientation variables $[{}^w x_0, {}^w y_0, \theta_0]$ relative to inertial frame system are chosen as the generalized coordinates. Besides, the passive joint J_4 is unactuated. Thus the rotation state φ_4 is chosen as an additional generalized coordinate. Integrally, the complete generalized coordinates of robotic fish are defined as $\boldsymbol{q} = [{}^w x_0, {}^w y_0, \theta_0, \varphi_4]^T$. Correspondingly, the generalized velocities $\dot{\boldsymbol{q}} = [{}^w \dot{x}_0, {}^w \dot{y}_0, \dot{\theta}_0, \dot{\varphi}_4]^T$ can be expressed. Then the Lagrangian function $L(\boldsymbol{q}, \dot{\boldsymbol{q}})$ is presented as follows:

$$L(\boldsymbol{q}, \dot{\boldsymbol{q}}) = T(\boldsymbol{q}, \dot{\boldsymbol{q}}) - E(\boldsymbol{q}), \tag{1}$$

where $T(\boldsymbol{q}, \dot{\boldsymbol{q}})$ and $E(\boldsymbol{q})$ denote the kinetic energy and potential energy, respectively. The kinetic energy is obtained by calculating the sum of translation and rotation kinetic energy of every links in the inertial coordinate system as follows:

$$T(\boldsymbol{q}, \dot{\boldsymbol{q}}) = \frac{1}{2} \sum_{i=0}^{4} \left({}^w v_i^T (M_i + M_i^a) {}^w v_i + {}^w \omega_i^T (I_i + I_i^a) {}^w \omega_i \right), \tag{2}$$

where, M_i and M_i^a are the mass matrix and additional mass matrix of i-th link, respectively. I_i and I_i^a are the inertia matrix and additional inertia matrix of i-th link, respectively.

As for the potential energy, the motion process of variable stiffness passive caudal fin is studied thoroughly. According to the passive joint diagram illustrated in Fig. 2, the conversion relationship between the passive joint rotation angle φ_4 and

the stretched length d_t of the passive tension spring can be derived as follows:

$$d_t = \sqrt{l_3^2 + l_{ps}^2 - 2l_3 l_{ps}\cos(\varphi_4)} - l_3 + l_{ps}, \tag{3}$$

where l_{ps} indicates the length of the crank, and l_3 represents the distance between joint J_4 and joint J_3.

With considering the pre-tension of the passive spring d_p, the elastic potential energy generated by the passive joint rotation can be expressed as follows:

$$E(\boldsymbol{q}) = K_t d_p d_t + \frac{1}{2} K_t d_t^2, \tag{4}$$

where K_t is the spring constant of the passive tension spring.

Then, a Lagrange formula of the second kind as (5) is employed to describe the dynamic model of the robotic fish.

$$\begin{cases} \dfrac{d}{dt}\dfrac{\partial L}{\partial^w \dot{x}_0} - \dfrac{\partial L}{\partial^w x_0} = F_x \\ \dfrac{d}{dt}\dfrac{\partial L}{\partial^w \dot{y}_0} - \dfrac{\partial L}{\partial^w y_0} = F_y \\ \dfrac{d}{dt}\dfrac{\partial L}{\partial^w \dot{\theta}_0} - \dfrac{\partial L}{\partial^w \theta_0} = \tau_0 \\ \dfrac{d}{dt}\dfrac{\partial L}{\partial^w \dot{\theta}_4} - \dfrac{\partial L}{\partial^w \theta_4} = \tau_4 \end{cases}. \tag{5}$$

where, F_x and F_y are the generalized external forces along axis x_w and y_w, respectively. τ_0 and τ_4 are the generalized external moments about axis z_0 and z_4, respectively. The external forces and moments are all generated by the the hydrodynamic forces.

B. Hydrodynamic Analysis

The external forces and moments are mainly generated by the added mass forces and the drag forces.

The added mass force is generated by the reaction of the fluid accelerating while the robotic fish swims. For the i-th link, the added mass is indicated as $M_{ia} = c_{ia} M_i$, the added mass force is indicated as $F_{a,i} = (F_{ax,i}, F_{ay,i}, F_{az,i})^T$ and it is relative to $O_w x_w y_w$. Thereby, the added mass force can be calculated as follows:

$$F_{a,i} = \begin{pmatrix} F_{ax,i} \\ F_{ay,i} \\ F_{az,i} \end{pmatrix} = -M_{ia} \begin{pmatrix} {}^w\dot{v}_{x,i} \\ {}^w\dot{v}_{y,i} \\ 0 \end{pmatrix}, \tag{6}$$

The drag force is generated from the friction viscosity and pressure difference caused by the robot motion. For the i-th link, the drag force is denoted as ${}^iF_{d,i} = ({}^iF_{dx,i}, {}^iF_{dy,i}, {}^iF_{dz,i})^T$ and is relative to $O_i - x_i y_i z_i$. By employing the simplified Morrison equation [25], the drag force ${}^iF_{d,i}$ is given as follows:

$${}^iF_{d,i} = \begin{pmatrix} {}^iF_{dx,i} \\ {}^iF_{dy,i} \\ {}^iF_{dz,i} \end{pmatrix} = \begin{pmatrix} -\frac{1}{2} c_{fi}\rho S_{x,i} |v_{x,i}| v_{x,i} \\ -\frac{1}{2} c_{di}\rho S_{y,i} |v_{y,i}| v_{y,i} \\ 0 \end{pmatrix}, \tag{7}$$

where c_{fi} and c_{di} are the friction coefficient and drag coefficient of the i-th link. ρ indicates the density of fluid. $S_{x,i}$ and $S_{y,i}$ are the characteristic areas in axis x_i and axis y_i. Moreover, the drag force $F_{d,i}$ expressed in $O_w - x_w y_w z_w$ can be obtained by transformation of coordinates.

On the basis of the above hydrodynamic analysis, the generalized force vectors are presented as follows:

$$\begin{pmatrix} F_x \\ F_y \\ F_z \end{pmatrix} = \sum_{i=0}^{4} F_{a,i} + \sum_{i=0}^{4} F_{d,i} \tag{8}$$

$$\begin{pmatrix} \tau_0 \\ \tau_4 \end{pmatrix} = \sum_{i=0}^{4} \begin{pmatrix} \tau_{a0,i} \\ \tau_{a4,i} \end{pmatrix} + \sum_{i=0}^{4} \begin{pmatrix} \tau_{d0,i} \\ \tau_{d4,i} \end{pmatrix}, \tag{9}$$

where $\tau_{a0,i}$ and $\tau_{d0,i}$ are the moments about axis z_0 produced by $F_{a,i}$ and $F_{d,i}$, respectively. Similarly, $\tau_{a4,i}$ and $\tau_{d4,i}$ are the moments about axis z_4 produced by $F_{a,i}$ and $F_{d,i}$, respectively.

Particularly, the hydrodynamic parameters involved in our research include the added mass coefficients c_{ma} and c_{Ia}, the friction coefficient c_{fi} of link L_i, and the drag coefficients c_{di} of link L_i. Because the links L_1-L_3 are similar in shape, we assume that they have same friction and drag coefficient to simplify the identification and are denoted as c_{f13} and c_{d13}, respectively.

In order to obtain practical values of the above hydrodynamic parameters, a data-driven identification method is applied. The proposed dynamic model is considered as a nonlinear gray-box model and the identification of hydrodynamic parameters is regarded as a process of optimization. In detail, the reference data are collected from the actual swimming experiments under different control parameters. The optimization objective is to minimize the standard deviation between the simulation data and experimental data. On the basis of above, the hydrodynamic parameters can be estimated by the optimization toolbox in MATLAB. Finally, with the complete presentation of external forces and torques, the four generalized variables can be resolved from the fourth equation in (5) as outputs of the proposed dynamic model.

IV. Locomotion Optimization of the Tendon-Driven Robotic Fish

Natural fish can achieve amazing swimming performance with the help of coordination between the body oscillation and the fins adjustment. For improving the performance of robotic fish, an optimization method including the asymmetric CPG model and the stiffness adjustment of the passive caudal fin is intensively studied in this section.

A. Improvement of the Asymmetric Hopf CPG Oscillator

For the quest of robotic fish mobility, the development of specific CPG model is researched firstly. Inspired by the behaviors of natural fishes, an accelerating factor is designed and

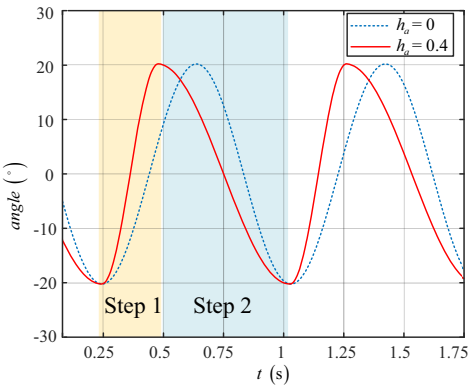

Fig. 4. The outputs of A-CPG model.

introduced to the traditional Hopf-CPG. Then, an improved asymmetric CPG (A-CPG) model is developed as follows:

$$\begin{cases} \dot{\alpha}_i = -\dfrac{1}{\zeta_i}\omega_i\left(\beta_i - b_i\right) + \alpha_i\left(A_i - \alpha_i^2 - \left(\beta_i - b_i\right)^2\right) \\ \dot{\beta}_i = \dfrac{1}{\zeta_i}\omega_i\alpha_i + \left(\beta_i - b_i\right)\left(A_i - \alpha_i^2 - \left(\beta_i - b_i\right)^2\right) \\ \zeta_i = 1 - h_{a,i}\dfrac{\dot{\alpha}_{pre,i}}{\left|\dot{\alpha}_{pre,i}\right|} \\ \varphi_i = h_{c,i}\alpha_i \end{cases}, \tag{10}$$

where α_i and β_i are the state variables of i-th CPG oscillator; ω_i, A_i, and b_i are the CPG parameters and stand for the frequency, amplitude, and bias of the output, respectively. $\dot{\alpha}_{pre,i}$ is the derivative of the state variable α_i at the previous moment. $h_{a,i}$ is the key asymmetric parameter of the oscillator. The improper value of $h_{a,i}$ may cause A-CPG instability and the speed of the servomotor is limited. Hence, the range of $h_{a,i}$ is limited to $[0, 0.8)$ to ensure a stable and practical asymmetric oscillator. Finally, $h_{c,i}$ is the constant parameter which is according to the mechanical structure. The outputs of A-CPG with different parameters are shown in Fig. 4, which control the bending angles of fish tail.

The A-CPG can be regarded as a state-space equation. It can be solved iteratively. Compared with the traditional symmetrical CPG, the introduction of the asymmetric parameter only changes the velocity of the limit cycle at different positions instead of the trajectory of the limit cycle. If $h_{a,i}$ is set to positive, the extra acceleration will be applied when $\dot{\alpha}_i > 0$, the extra deceleration will be applied in the other phase. With the acceleration and deceleration in the different phases, the output of A-CPG is asymmetric. In this way, the proposed A-CPG can achieve different tail-beat speeds in one period as Fig. 4. In step 1, the tail beats to one side at a faster speed. In step 2, the tail goes back to the other side at a slower speed. The higher beating speed can generate a bigger hydrodynamic force to rotate robotic fish. When the tail-beat speeds of two steps are different, the asymmetric force will act on the robotic fish and result in the improvement of the steering.

B. Adjustment Regulation of the Passive Joint

By further considering the variable stiffness passive caudal fin presented in Section II, the torque acted on J_4 caused by passive spring can be derived as follows:

$$\tau_p = F\sin\left(\varphi_4 + \cos\frac{l_3 - l_{cr,3}}{d_t}\right)l_{cr,3}, \tag{11}$$

where d_t is spring elongation caused by rotation and can be derived following (3). F is the total tension of the spring and can be calculated as $F = k_t\left(d_t + d_p\right)$. It can be seen that the total tension is generated from two elongation. The elongation d_t can be calculated by (3). The elongation d_p can be adjusted by the stiffness adjustment servomotor. Under the same passive rotation angle φ_4, the passive torque is mainly dominated by the pre-tension d_p, which can be considered as adjustable stiffness.

In order to find an appropriate passive stiffness adjustment rule, we develop two reasonable hypotheses. Firstly, the passive stiffness remains constant under the same swimming velocity. Secondly, the swimming velocity is determined only by the tail-beat amplitude and frequency. In these cases, the passive stiffness can be adjusted according to the A-CPG parameters.

For the above purpose, the problem of stiffness adjustment is considered as a multi-objective optimization problem (MOP), and the robotic fish model is indicated as $[V, \Omega] = \mathcal{G}(d_p|A, f)$. The objectives of stiffness adjustment are to improve the maneuverability and stability of robotic fish. The forward swimming velocity and yaw oscillation velocity are the main embodiments of the above targets. Hence, the forward velocity V and the yaw angular velocity Ω chosen as the main variables to be optimized. A and f are the tail-beat amplitude and frequency, which are controllable. d_p is the pre-tension of passive spring. In order to obtain a proper d_p to achieve faster and more steady swimming performance, two loss functions $[F_1, F_2]$ are designed as follows:

$$\begin{aligned} F_1 &= -\frac{1}{N}\sum_{i=0}^{N} V_i \\ F_2 &= \max(\Omega_i) - \min\left(\Omega_i\right) \end{aligned}, \tag{12}$$

where V_i and Ω_i are the forward velocity and the yaw angular velocity, N is the length of the data. F_1 is related to the forward velocity. The greater steady forward swimming velocity and shorter velocity convergence time can generate

Algorithm 1 Design of passive stiffness adjustment

```
Discretize the amplitude as 𝒜;
Discretize the frequency as ℱ;
Initialize the boundary and initial value of d_p;
for each A ∈ 𝒜 do
    for each f ∈ ℱ do
        Solve MOP by NSGA-II;
        Record the optimized result d_p and the current frequency;
    end for
    Fit d_p as function about frequency;
    Record the stiffness adjustment rule as d_p = g_A(f);
end for
Output d_p = g_A(f), A ∈ 𝒜;
```

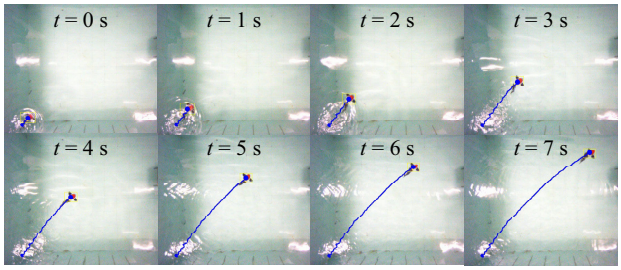

Fig. 5. Snapshot sequence of robotic fish forward swimming.

TABLE II
PHYSICAL PARAMETERS OF THE DYNAMIC MODEL

Items	Unit	L0	L1	L2	L3	L4
m_i	kg	2.133	0.081	0.081	0.081	0.096
I_i	g·m^2	91.6	0.23	0.23	0.21	0.29
l_i	m	0.270	0.032	0.032	0.032	0.100
l_{ci}	m	0.192	0.016	0.016	0.016	0.027
$S_{x,i}$	cm^2	289.09	90.47	90.99	86.21	68.53
$S_{y,i}$	cm^2	127.27	92.89	57.22	37.96	10.79

a smaller loss value. F_2 is employed to maintain swimming stability and the smaller oscillation amplitude in yaw DOF will obtain a smaller loss value. By minimizing the designed loss functions, the pre-tension of passive spring corresponding to a set of amplitude and frequency can be obtained.

Then, the amplitude A and the frequency f are discretized for simplifying optimization. In detail, A is discretized in step of 5° within the range of [15°, 35°] and f is discretized in step of 0.2 Hz within the range of [0.6 Hz, 2.0 Hz]. Under a set of [A, f], the corresponding pre-tension of passive spring can be obtained by minimizing the loss functions.

In this paper, the non-dominated sorting genetic algorithm (NSGA-II) [33] is applied to solve the above optimization problem. Based on the loss functions $[F_1, F_2]$, NSGA-II can return a set of Pareto solutions including the anticipated solution. In summary, the optimization of passive stiffness adjustment can be accomplished following the pseudo-code Algorithm 1.

V. Simulations and Experiments

In this section, extensive simulations and aquatic experiments are carried out to verify the proposed motion optimization methods. Experiments are conducted in a water tank with a size of 5 m × 4 m × 1.2 m. A global camera that is mounted above the tank is applied to measure the motion states of the robotic fish, and the detail of motion measurement can refer to our previous work [34]. Fig. 5 shows the snapshot sequence captured by the global camera, and motion states are estimated through the color marks.

A. Dynamic Model Identification and Validation

Regarding the model parameters, some physical parameters can be measured or calculated easily by SolidWorks, as listed in Table II. For estimating the hydrodynamic parameters, the reference data is obtained by experiments with different control parameters. Based on the reference data and the optimization toolbox, the estimated hydrodynamic parameters are given in Table III. Besides, the optimization boundaries $[\lambda_{min}, \lambda_{max}]$ and the initial values λ_0 are also tabulated in Table III.

TABLE III
HYDRODYNAMIC PARAMETERS OF THE DYNAMIC MODEL

Items	λ_{min}	λ_{max}	λ_0	λ
c_{ma}	0	3	1.5	1.15971
c_{Ia}	0	3	1.5	1.30205
$c_{d,0}$	0	5	2.5	4.88539
$c_{d,13}$	0	5	2.5	0.14055
$c_{d,4}$	0	6	3.0	5.76034
$c_{f,0}$	0	1	0.5	0.01229
$c_{f,13}$	0	1	0.5	0.01005
$c_{f,4}$	0	1	0.5	0.01020

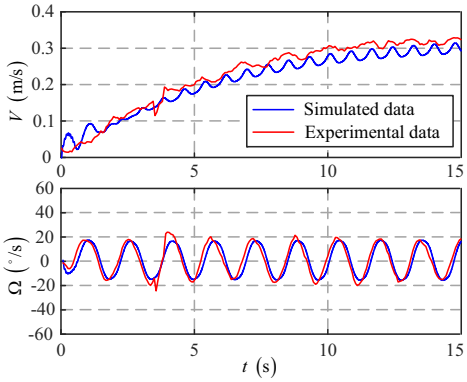

Fig. 6. The comparison of the experimental data and simulated data of dynamic model under the control parameter of A = 20° and f = 0.7 Hz.

To verify the proposed dynamic model and the estimated model parameters, the forward velocity V and yaw angular velocity Ω are mainly focused. Fig. 6 shows the comparison of transient states between simulation results and actual experiment results. Intuitively, the motion states of simulation can match well with the actual experiment either in acceleration or steady swimming phase. Notice there is a significant change in angular velocity at around 4 s. This is due to a measurement error caused by the color label detection failure. Further, the root-mean-square error (RMSE) $[E_V, E_\Omega]$ is applied to assess the model accuracy of forward velocity and yaw angular velocity. Besides, the corresponding normalized RMSE $[\overline{E_V}, \overline{E_\Omega}]$ is calculated, which can evaluate the model accuracy more intuitively [8], [35]. In detail, the errors can be calculated following (13) and (14), respectively.

$$\begin{cases} E_V = \sqrt{\dfrac{1}{N}\sum_{i=0}^{N}\left(V_e\left(i\right) - V_s\left(i\right)\right)^2} \\ \overline{E_V} = E_V / \left(\max\left(V_e\right) - \min\left(V_e\right)\right) \end{cases}, \tag{13}$$

$$\begin{cases} E_\Omega = \left|\max\left|\Omega_e\right| - \max\left|\Omega_s\right|\right| \\ \overline{E_\Omega} = E_\Omega / \max\left|\Omega_e\right| \end{cases}, \tag{14}$$

TABLE IV
FITTING ERRORS OF SIMULATION RESULTS

Mode (f(Hz), $A(^\circ)$)	E_V (m/s)	$\overline{E_V}$	E_Ω ($^\circ$/s)	$\overline{E_\Omega}$
$f = 1.0, A = 20$	0.019	0.091	0.816	0.029
$f = 1.0, A = 30$	0.016	0.053	1.186	0.028
$f = 1.4, A = 30$	0.019	0.070	0.390	0.014
$f = 1.4, A = 30$	0.016	0.053	1.186	0.049
$f = 1.8, A = 20$	0.028	0.076	1.198	0.034
$f = 1.8, A = 30$	0.046	0.069	1.856	0.054
Max error	0.046	0.091	1.856	0.054
Mean error	0.024	0.068	1.105	0.034

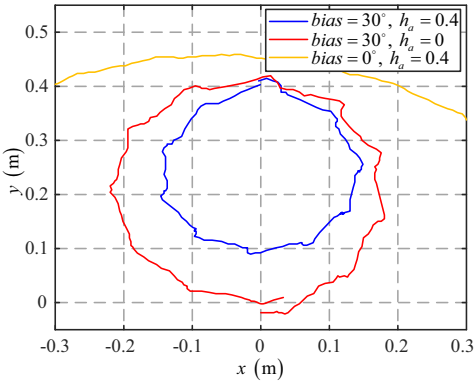

Fig. 7. Experimental swimming trajectories with different biases and control modes. The uniform tail-beat frequency is $f = 0.8$ Hz.

where V_e and V_s are the experiment data sequences and dynamic simulation data sequences, respectively. With a set of control modes, experiments and simulations are carried out and the corresponding errors are calculated as Table IV. In Table IV, each indicator has a set of corresponding values under different Mode. The "Max error" is the maximum of each set of errors. The "Mean error" is the average of the each set of errors. The slight simulation errors show that the proposed dynamic model can fit well with the actual motion states under multiple tail-beat frequency and amplitude. The mean normalized RMSEs are calculated as 6.8% and 3.4%, respectively, which is a demonstration of the validity of proposed dynamic model.

B. Steering Motion Experiments with A-CPG

For verifying the performance improvement bought by A-CPG, a set of steering experiments are implemented. Swimming trajectories with different control modes are plotted in Fig. 7. When the A-CPG is applied and the offset is set to 0, the robotic fish can turn steadily. It demonstrates that the asymmetric tail-beat can generate rotation torque in yaw DOF. Besides, combined with the beat offset, the steering radius is reduced obviously with the application of A-CPG. To further study the performance improvement of A-CPG and its reasons, the yaw angle curves in one period are shown in Fig. 8. In one turning period, the positive and negative rotation show an obvious asymmetry. Under the larger tail-beat offset, the steering angle is improved effectively. Under the smaller tail-beat offset, the improvement in steering angle is relatively weak but the reduction in the reverse steering is still significant. Besides, the quantitative experiments are carried out with f = 1 Hz and h_a = 0.4, and valuable indicators based on different biases and control modes are calculated as listed in Table V. For the involved indicators, R is the steering radius. ξ is the difference between yaw angle peaks as indicated in Fig. 8, which can reflect the degree of steering stability. ω_{max} and $\bar{\omega}$ are the maximum steering angular velocity and mean steering angular velocity in one period.

TABLE V
STEERING RESULTS WITH DIFFERENT CONTROL MODES AND PARAMETERS

$Bias$ ($^\circ$)	Mode	R (m)	ξ ($^\circ$)	ω_{max} ($^\circ$/s)	$\bar{\omega}$ ($^\circ$/s)
25	CPG	0.44	26.9	96.2	17.3
	A-CPG	0.45	19.8	119.1	17.1
30	CPG	0.44	30.4	80.8	37.3
	A-CPG	0.3	21.2	118.5	41.2
35	CPG	0.22	28.4	133.2	24.7
	A-CPG	0.14	21.1	153.3	30.9

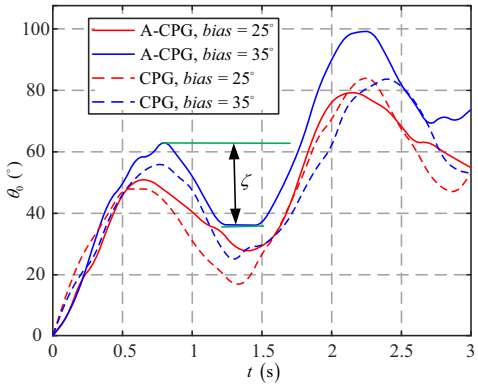

Fig. 8. Comparative results of yaw angle between CPG and A-CPG in turning cycle. The uniform control parameters are $A = 30^\circ$ and $f = 0.8$ Hz.

Compared with the traditional CPG, the steering radius is reduced and the stability of the steering motion is improved effectively. With the proposed A-CPG, the steering radius reduces from 0.22 m to 0.14 m, and the reduction is 36.3%. ξ reduces from 30.4° to 21.2°. The improvement of steering stability is 30.2%. With the aid of A-CPG, the maximum steering angular velocity and minimum steering radius reach 153.3°/s and 0.31 BL, respectively. Notice that the improvement is not significant when $A = 25^\circ$. When $A = 25^\circ$, the amplitude of tail is relatively small. In this case, the acceleration phase of A-CPG is short. The duration of the two asymmetric phase is similar. As a result, the hydrodynamic forces in the two phases are similar and the advantages of A-CPG are not obvious.

C. Experiments of Passive Stiffness Adjustment

Following the designed optimization algorithm of passive stiffness adjustment presented in Section IV, the pre-tension about frequency is fitted as quadratic functions and illustrated in Fig. 9.

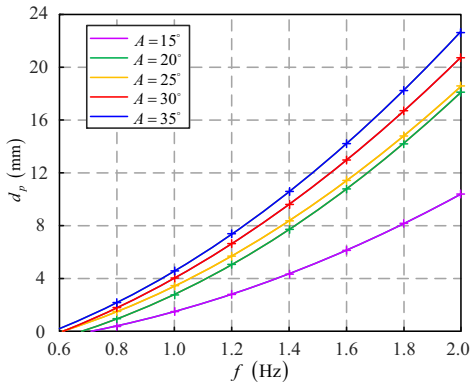

Fig. 9. The optimized passive stiffness adjustment rules obtained by Algorithm 1.

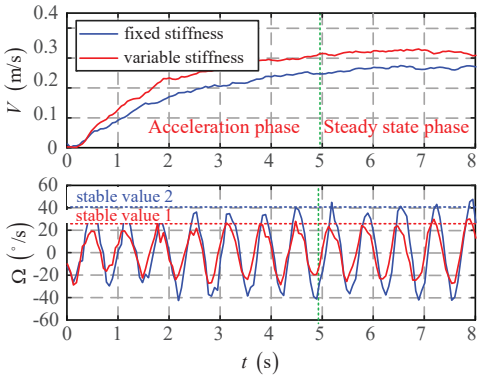

Fig. 10. Comparison of forward swimming experiments between fixed passive stiffness and variable passive stiffness. The other control parameters are $A = 20°$ and $f = 1.5$ Hz.

Under the same A-CPG parameter, the forward swimming experiments are carried out with fixed and variable stiffness passive caudal fin. The motion states are illustrated in Fig. 10. Because of the waves reflected by the pool walls, there are some uneven changes of angular velocity. But the overall contrast is still stark. It can be seen that the swimming velocity is improved effectively. Besides, the maximum yaw angular velocity with the variable stiffness (stable value 2 in Fig. 10) is significantly reduced compared with angular velocity with fixed stiffness (stable value 1 in Fig. 10). It reflects that the variable stiffness of passive joint can maintain the optimal shape of robotic fish, so as to make energy focus on propelling the robotic fish forward rather than swinging its head. Under the concern of forward swimming velocity, a set of comparative experiments about passive stiffness at different frequencies are implemented, where the variable stiffness is obtained through adjustment rule and the pre-tensions for comparison are fixed to 30 mm. The steady state velocities under different conditions are recorded and shown in Fig. 11. It is obvious that variable stiffness passive caudal fin can provide performance improvements at multiple tail-beat amplitudes and frequencies, especially in the high frequency band. With the variable stiffness passive caudal fin, the maximum forward swimming velocity improves from 0.32 m/s to 0.45 m/s. The improvement is 29%. Finally, current version of tendon-driven robotic fish reaches the maximum velocity of 0.47 m/s (1.04 BL/s) at f = 2.2 Hz and A = 35°. This is also an important verification of the rationality of mechanism design and the effectiveness of motion optimization methods.

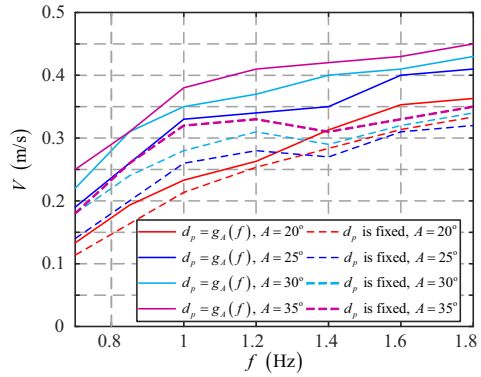

Fig. 11. Experimental forward swimming velocity under difference amplitudes and pre-tensions.

D. Discussion

Based on simulations and actual experiments, the superiority of proposed motion optimization methods based on "T-Fish" are well proven. For optimization and methods validation, the Lagrange modeling method and data-driven parameters identification method are presented to establish the dynamic model of "T-Fish". According to the comparison of simulations and experiments, the mean NRMSE of forward swimming velocity and yaw angular velocity are 6.8% and 3.4%, respectively. It lays the foundation for motion optimization.

For the improvement on the steering motion and forward velocity, the asymmetric CPG and entire variable stiffness passive caudal fin system are implemented. With the developed A-CPG, the steering mobility is enhanced effectively. The minimum turning radius and peak turning speed reach 0.31 BL and 153.3°/s, respectively. Furthermore, the variable stiffness passive caudal fin system significantly improves the forward swimming velocity. The maximum swimming velocity reaches 1.04 BL/s with 2.2 Hz and the maximum speed increase is up to 29% by applying the stiffness adjustment rule. According to the comparison with the similar bionic robotic fishes as listed in Table VI, the developed robotic fish shows advantages in both swimming velocity and steering maneuver. According to the swimming velocity experiment, the maximum swimming velocity is limited by the tail-beat frequency and the hydraulic resistance. Hence the optimization on transmission mechanism the shape of the robotic fish is still an issue.

VI. Conclusion and Future Works

In this paper, we have developed a new type tendon-driven robotic fish with a variable stiffness passive caudal fin. Based on the developed prototype, a set of locomotion optimization methods are explored. First, we design a dual tendon driving active tail and variable stiffness passive caudal fin for better performance and stability. Second, considering the active tail

TABLE VI
PERFORMANCE COMPARISON OF ROBOTIC FISHES

Robotic fishes	Frequency (Hz)	Maximum velocity (BL/s)	Steering radius (BL)
Wire-driven robotic shark [11]	2	0.22	–
Tensegrity robotic fish [12]	1.5	0.58	–
Soft robotic fish [13]	1.4	0.5	1.66
Wire-driven robotic fish [15]	3	2.15	–
Wire-driven robotic fish [14]	3	0.67	0.7
Our robotic fish	**2.2**	**1.04**	**0.31**

and compliant part, a practical dynamic model for the tendon-driven robotic fish is established, where the hydrodynamic parameters are obtained based on a data-driven identification method. Third, we propose a set of locomotion optimization methods including an asymmetric central pattern generator and an adjustment rule of passive stiffness, which can effectively improve the steering and forward swimming performances. Finally, extensive simulations and aquatic experiments are carried out to validate the effectiveness of the proposed prototype and methods. The obtained results indicate that the improvements in steering radius and forward swimming velocity are 36.3% and 29%, respectively. The proposed robotic fish can achieve maximum forward swimming as 1.04 BL/s, maximum turning rate as 153.3°/s, and the minimum turning radius reaches 0.31 BL, which offers valuable insight into fish-like robots.

In the future, we will focus on the system optimization and morphology-related hydrodynamic studies to further enhance the performance of the robotic fish. Meanwhile, the ocean mission-oriented motion control based on intelligent methods will also be an important concern.

REFERENCES

[1] J. Yu, M. Wang, H. Dong, Y. Zhang, and Z. Wu, "Motion control and motion coordination of bionic robotic fish: A review," *J. Bionic Eng.*, vol. 15, no. 4, pp. 579–598, Jul. 2018.

[2] F. E. Fish, "Advantages of natural propulsive systems," *Mar. Technol. Soc. J.*, vol. 47, no. 5, pp. 37–44, Oct. 2013.

[3] M. Triantafyllou and G. Triantafyllou, "An efficient swimming machine," *Sci. Amer.*, vol. 272, no. 3, pp. 64–70, Mar. 1995.

[4] S. Zhang, Y. Qian, P. Liao, F. Qin, and J. Yang, "Design and control of an agile robotic fish with integrative biomimetic mechanisms," *IEEE/ASME Trans. Mechatronics*, vol. 21, no. 4, pp. 1846–1857, Aug. 2016.

[5] L. Wen, T. Wang, G. Wu, J. Liang, and C. Wang, "Novel method for the modeling and control investigation of efficient swimming for robotic fish," *IEEE Trans. Ind. Electron.*, vol. 59, no. 8, pp. 3176–3188, Aug. 2012.

[6] X. Tan, "Autonomous robotic fish as mobile sensor platforms: Challenges and potential solutions," *Mar. Technol. Soc. J.*, vol. 45, no. 4, pp. 31–40, Aug. 2011.

[7] Z. Wu, J. Liu, J. Yu, and H. Fang, "Development of a novel robotic dolphin and its application to water quality monitoring," *IEEE/ASME Trans. Mechatronics*, vol. 22, no. 5, pp. 2130–2140, Oct. 2017.

[8] T. Aritani, N. Kawasaki, and Y. Takada, "Small robotic fish with two magnetic actuators for autonomous tracking of a goldfish," *J. Aero. Aqua. Bio-mech.*, vol. 8, no. 1, pp. 69–74, Aug. 2019.

[9] Q. Shen, T. Wang, L. Wen, and J. Liang, "Modelling and fuzzy control of an efficient swimming ionic polymer-metal composite actuated robot," *Int. J. Adv. Robot. Syst.*, vol. 10, no. 10, pp. 350–363, Jul. 2013.

[10] M. Sfakiotakis, D. Lane, and J. Davies, "Review of fish swimming modes for aquatic locomotion," *IEEE J. Ocean. Eng.*, vol. 24, no. 2, pp. 237–252, Apr. 1999.

[11] W. Lau, Y. Zhong, R. Du, and Z. Li, "Bladderless swaying wire-driven robot shark," in *Proc. Int. Conf. Robot. Autom. Mech.*, Siem Reap, Cambodia, Jul. 2015, pp. 155–160.

[12] J. Shintake, D. Zappetti, T. Peter, Y. Ikemoto, and D. Floreano, "Bio-inspired tensegrity fish robot," in *Proc. Int. Conf. Robot. Autom.*, Paris, France, Aug. 2020, pp. 2887–2892.

[13] R. Katzschmann, J. DelPreto, R. MacCurdy, and D. Rus, "Exploration of underwater life with an acoustically controlled soft robotic fish," *Sci. Robot.*, vol. 3, no. 16, pp. 3449–3461, Mar. 2018.

[14] Y. Zhong, Z. Li, and R. Du, "The design and prototyping of a wire-driven robot fish with pectoral fins," in *Proc. IEEE Int. Conf. Robot. Biomim.*, Shenzhen, China, Dec. 2013, pp. 1918–1923.

[15] Y. Zhong, Z. Li, and R. Du, "A novel robot fish with wire-driven active body and compliant tail," *IEEE/ASME Trans. Mechatronics*, vol. 22, no. 4, pp. 1633–1643, Aug. 2017.

[16] J, Liu, C. Zhang, Z. Liu, R. Zhao, D. An, Y. Wei, Z. Wu, and J. Yu, "Design and analysis of a novel tendon-driven continuum robotic dolphin," *Bioinspir. Biomim.*, vol. 16, no. 6, Art. no. 065002, Sep. 2021.

[17] Z. Li, Y. Zhong, and R. Du, "A novel underactuated wire-driven robot fish with vector propulsion," in *Proc. Int. Conf. Intell. Robot. Syst.*, Tokyo, Japan, Nov. 2013, pp. 941–946.

[18] A. J. Ijspeert, A. Crespi, D. Ryczko, and J. Cabelguen, "From swimming to walking with a salamander robot driven by a spinal cord model," *Sci.*, vol. 315, no. 5817, pp. 1416–1420, Mar. 2007.

[19] X. Niu, J. Xu, Q. Ren, and Q. Wang, "Locomotion learning for an anguilliform robotic fish using central pattern generator approach,' *IEEE Trans. Ind. Electron.*, vol. 61, no. 9, pp. 4780-4787, Sep. 2014.

[20] Y. Hu, J. Liang, and T. Wang, "Parameter synthesis of coupled non-linear oscillators for CPG-based robotic locomotion," *IEEE Trans. Ind. Electron.*, vol. 61, no. 11, pp. 6183–6191, Nov. 2014.

[21] Z. Wu, J. Yu, Z. Su, M. Tan, and Z. Li, "Towards an esox lucius inspired multimodal robotic fish," *Sci. China Inform. Sci.*, vol. 58, no. 5, pp. 1–13, May 2015.

[22] Z. Su, J. Yu, M. Tan, and J. Zhang, "Implementing flexible and fast turning maneuvers of a multijoint robotic fish," *IEEE/ASME Trans. Mechatronics*, vol. 19, no. 1, pp. 329–338, Feb. 2014.

[23] A. D. Marchese, C. D. Onal, and D. Rus, "Autonomous soft robotic fish capable of escape maneuvers using fluidic elastomer actuators," *Soft Robot.*, vol. 1, no. 1, pp. 329–338, Mar. 2014.

[24] G. V. Lauder, E. J. Anderson, J. Tangorra, and P. G. A. Madden, "Fish biorobotics: Kinematics and hydrodynamics of self-propulsion," *Journal of experimental biology*, vol. 215, no. 1, pp. 56–67, Jan. 2012.

[25] D. Chen, Z. Wu, H. Dong, M. Tan, and J. Yu, "Exploration of swimming performance for a biomimetic multi-joint robotic fish with a compliant passive joint," *Bioinspir. Biomim.*, vol. 16, no. 2, Art. no. 026007, Dec. 2020.

[26] P. L. Nguyen, B. R. Wu, and K. K. Ahn, "Thrust and swimming speed analysis of fish robot with non-uniform flexible tail," *J. Bionic Eng.*, vol. 13, no. 1, pp. 73–83, Jan. 2016.

[27] S. B. Behbahani and X. Tan, "Design and modeling of flexible passive rowing joint for robotic fish pectoral fins," *IEEE Trans. Robot.*, vol. 32, no. 5, pp. 1119–1132, Oct. 2016.

[28] Y. Park, T. Huh, D. Park, and K. Cho, "Design of a variable-stiffness flapping mechanism for maximizing the thrust of a bio-inspired underwater robot," *Bioinspir. Biomim.*, vol. 9, no. 3, Art. no. 036002, Mar. 2014.

[29] Y. Park, U. Jeong, J. Lee, S. Kwon, H. Kim, and K. Cho, "Kinematic condition for maximizing the thrust of a robotic fish using a compliant caudal fin," *IEEE Trans. Robot.*, vol. 28, no. 6, pp. 1216–1227, Dec. 2012.

[30] Q. Zou, B. Lu, Y. Fu, X. Liao, Z. Zhang, and C. Zhou, "Dynamic modeling and optimization of robotic fish based on passive flexible mechanism," in *Proc. IEEE Int. Conf. Mech. Autom.*, Takamatsu, Japan, Aug. 2021, pp. 622–627.

[31] B. Chen and H. Jiang, "Body stiffness variation of a tensegrity robotic fish using antagonistic stiffness in a kinematically singular configuration," *IEEE Trans. Robot.*, vol. 37, no. 5, pp. 1712–1727, Oct. 2021.

[32] Q. Zhong, J. Zhu, F. E. Fish, S. J. Kerr, A. M. Downs, H. Bart-Smith, and D. B. Quinn, "Tunable stiffness enables fast and efficient swimming in fish-like robots," *Sci. Robot.*, vol. 6, no. 57, pp. 4088–4097, Aug. 2021.

[33] K. Deb, A. Pratap, S. Agarwal, and T. Meyarivan, "A fast and elitist multiobjective genetic algorithm: NSGA-II," *IEEE Trans. Evol. Comput.*, vol. 6, no. 2, pp. 182–197, Apr. 2002.
[34] J. Yuan, J. Yu, Z. Wu, and M. Tan, "Precise planar motion measurement of a swimming multi-joint robotic fish," *Sci. China Inform. Sci.*, vol. 59, no. 9, pp. 1–15, Aug. 2016.
[35] V. Kopman, J. Laut, F. Acquaviva, A. Rizzo, and M. Porfiri, "Dynamic modeling of a robotic fish propelled by a compliant tail," *IEEE J. Ocean. Eng.*, vol. 40, no. 1, pp. 209–221, Jan. 2015.

Changlin Qiu received the B.E. degree in automation from the School of Control Science and Engineering, Shandong University, Jinan, China, in 2019. He is currently pursuing the Ph.D. degree in control theory and control engineering from the Institute of Automation, Chinese Academy of Sciences, Beijing, China.

His current research interests include underwater robotics and intelligent control systems.

Zhengxing Wu received the B.E. degree in logistics engineering from the School of Control Science and Engineering, Shandong University, Jinan, China, in 2008, and the Ph.D. degree in control theory and control engineering from the Institute of Automation, Chinese Academy of Sciences (IACAS), Beijing, China, in 2015.

He is currently a Professor with the State Key Laboratory of Management and Control for Complex Systems, IACAS. His research interests include fast maneuvers of bioinspired robotic fish and gliding motions of robotic dolphins.

Jian Wang received the B.E. degree in automation from University of Science and Technology Beijing, Beijing, China, in 2016, and the Ph.D. degree in control theory and control engineering from the Institute of Automation, Chinese Academy of Sciences (IACAS), Beijing, China, in 2021.

He is currently an Assistant Professor with the State Key Laboratory of Management and Control for Complex Systems, IACAS. His research interests include bioinspired underwater robots and intelligent control systems.

Min Tan received the B.Sc. degree from Tsinghua University, Beijing, China, in 1986, and the Ph.D. degree from the Institute of Automation, Chinese Academy of Sciences (IACAS), Beijing, China, in 1990, both in control science and engineering. He is currently a Professor with the State Key Laboratory of Management and Control for Complex Systems, IACAS. He has published more than 200 papers in journals, books, and conference proceedings.

His research interests include robotics and intelligent control systems.

Junzhi Yu (Fellow, IEEE) received the B.E. degree in safety engineering and the M.E. degree in precision instruments and mechanology from the North University of China, Taiyuan, China, in 1998 and 2001, respectively, and the Ph.D. degree in control theory and control engineering from the Institute of Automation, Chinese Academy of Sciences, Beijing, China, in 2003.

From 2004 to 2006, he was a Postdoctoral Research Fellow with the Center for Systems and Control, Peking University, Beijing. In 2006, he was an Associate Professor with the Institute of Automation, Chinese Academy of Sciences, where he became a Full Professor in 2012. In 2018, he joined the College of Engineering, Peking University, as a Tenured Full Professor. His current research interests include intelligent robots, motion control, and intelligent mechatronic systems.